Measurement of Tensor Polarization in Elastic Electron-Deuteron Scattering in the Momentum-Transfer Range $3.8 \leq q \leq 4.6$ fm^{-1}

I. The,[6] J. Arvieux,[5] D. H. Beck,[2,8] E. J. Beise,[6] A. Boudard,[3] E. B. Cairns,[1] J. M. Cameron,[1,4] G. W. Dodson,[6] K. A. Dow,[6] M. Farkhondeh,[6] H. W. Fielding,[1] J. B. Flanz,[6] M. Garçon,[3,6] R. Goloskie,[9] S. Høibråten,[6] J. Jourdan,[2] S. Kowalski,[6] C. Lapointe,[1] W. J. McDonald,[1] B. Ni,[4] L. D. Pham,[6] R. P. Redwine,[6] N. L. Rodning,[1] G. Roy,[1] M. E. Schulze,[7] P. A. Souder,[7] J. Soukup,[1] W. E. Turchinetz,[6] C. F. Williamson,[6] K. E. Wilson,[6] S. A. Wood,[6,8] and W. Ziegler[1]

[1]*University of Alberta, Edmonton, Alberta, Canada T6G 2N5*
[2]*California Institute of Technology, Pasadena, California 91125*
[3]*Département de Physique Nucléaire-Saclay, 91191 Gif-sur-Yvette, France*
[4]*Indiana University Cyclotron Facility, Bloomington, Indiana 47405*
[5]*Laboratoire National Saturne, 91191 Gif-sur-Yvette, France*
[6]*Massachusetts Institute of Technology, Cambridge, Massachusetts 02139*
[7]*Syracuse University, Syracuse, New York 13210*
[8]*University of Illinois, Champaign, Illinois 61820*
[9]*Worcester Polytechnic Institute, Worcester, Massachusetts 01609*

(Received 11 March 1991; revised manuscript received 28 May 1991)

The tensor polarization t_{20} of the recoil deuteron in elastic *e-d* scattering has been measured for three values of four-momentum transfer, $q = 3.78$, 4.22, and 4.62 fm^{-1}. The data have been used to locate the first node in the charge monopole form factor of the deuteron at $q = 4.39 \pm 0.16$ fm^{-1}. The results for t_{20} are in reasonable agreement with expectations based on the nucleon-meson description of nuclear dynamics.

PACS numbers: 25.30.Bf, 24.70.+s, 25.10.+s, 27.10.+h

The electromagnetic structure of the spin-1 deuteron is described by three form factors: charge monopole F_C, charge quadrupole F_Q, and magnetic dipole F_M. Cross-section measurements in elastic *e-d* scattering yield the structure functions $A(F_C, F_Q, F_M)$ and $B(F_M)$ [1] but do not allow the separation of F_C and F_Q. Therefore, the measurement of another observable is necessary. We have measured the tensor polarization of the recoil deuteron [2]:

$$t_{20} = -\sqrt{2}[x(x+2)+y/2]/[1+2(x^2+y)], \quad (1)$$

where $x = \frac{2}{3}\eta F_Q/F_C$, $y = \frac{2}{3}\eta f(\theta_e)F_M^2/F_C^2$, $f(\theta_e) = \frac{1}{2} + (1+\eta)\tan^2(\theta_e/2)$, and $\eta = q^2/4M_d^2$; q is the four-momentum transfer, M_d is the deuteron mass, and θ_e is the electron-scattering angle in the laboratory frame. The quantity $\tilde{t}_{20} \equiv t_{20}(y=0)$, derived from Eq. (1) by neglecting the magnetic contribution, is often used in the literature. The measurements reported here cover a q range $3.8 \leq q \leq 4.6$ fm^{-1} where the short-distance structure of the deuteron and non-nucleonic degrees of freedom are expected to become important. Previous measurements [3–5] of t_{20} have been reported at lower momentum transfers. F_C is particularly sensitive to model variations in the q range $3 < q < 6$ fm^{-1}, where it is generally expected to pass through zero, while F_Q, which largely determines the cross section in this q range, is less sensitive to the details of various models.

The experiment was performed at the Massachusetts Institute of Technology–Bates Linear Accelerator Center. Figure 1 shows a layout of the experimental arrangement. The electron beam from the linac was used at energies of 653, 755, and 853 (± 3) MeV, with an average current between 5 and 30 μA and a duty cycle of about 0.8%. It was incident on a 7-cm-long liquid-deuterium target. The recoil deuterons were selected in a specially designed magnetic channel, fixed at an angle of 41°, consisting of a quadrupole-quadrupole-dipole (QQD), an intermediate focus detection (IFD), and a quadrupole-quadrupole-quadrupole-dipole (QQQD) system. The scattered electrons were analyzed with a magnetic spectrometer (OHIPS), having a solid angle of 18 msr. The angle of OHIPS for each q point is given in Table I. The q values and their uncertainties, due to the uncertainties in the electron-beam energies and OHIPS angles ($\pm 0.1°$), are also given in Table I. The IFD was composed of two multiwire proportional chambers (MWPC's) used for tuning only and a hodoscope of ten scintillators. The "Alberta high efficiency analyzer for deuterons" (AHEAD) was installed in a shielded hut at the end of the deuteron channel. For the runs taken at the two higher electron energies, a carbon degrader was installed in front of the hodoscope. This degrader was used to reduce the flux of protons entering the polarimeter and to lower the deuteron energies to values within the maximum efficiency range of AHEAD. The coincidence between OHIPS, IFD, and AHEAD led to an unambiguous identification of *e-d* elastic events.

The polarimeter was based on *d-p* elastic scattering [6]. In the deuteron energy range of interest (60–170 MeV), the angular distribution of the analyzing power

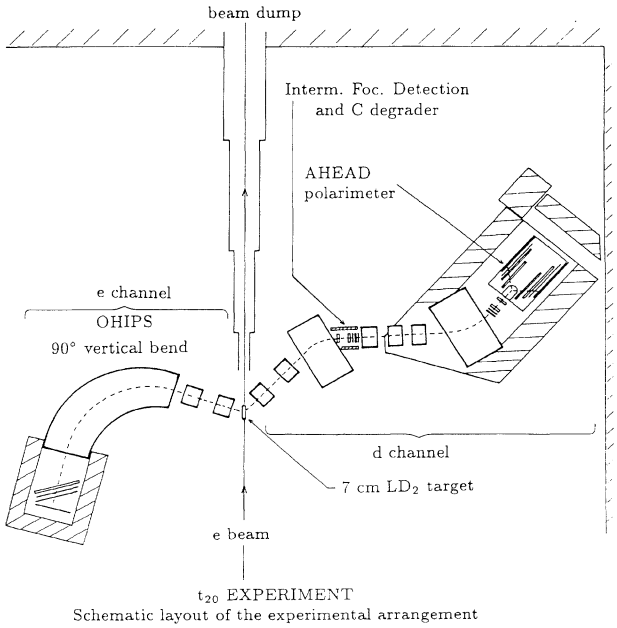

FIG. 1. The electron channel: QQD, three plastic scintillators, and a drift chamber. The deuteron channel: QQD, IFD and carbon degrader, and QQQD.

T_{20} exhibits a characteristic minimum ($T_{20}\simeq -0.45$) at $\theta_{\text{c.m.}}\simeq 115°$ and a maximum ($T_{20}\simeq 0.3$) at $\theta_{\text{c.m.}}\simeq 150°$. The deuterons from *e-d* elastic-scattering events were incident upon a 27-cm-long liquid-hydrogen (LH_2) target with a 10-cm diameter. Their incident trajectories were determined by two MWPC's triggered by two scintillators in front of the MWPC's. Two cylindrical wire chambers (CWC's), positioned concentrically around the LH_2 target, were used to measure the polar and azimuthal angles of the scattered particles. The CWC's were surrounded by an array of six ΔE (150 cm×22 cm×0.3 cm) and eighteen E plastic scintillators (7.6 cm thick) to measure the energies of detected particles and identify them through their energy losses. The polarimeter was calibrated with a deuteron beam of known polarization at the Laboratoire National Saturne [7]. More detailed descriptions of the polarimeter and the analysis of the calibration data will be published [8] elsewhere.

The calibration runs relevant to this experiment were performed at 120, 145, and 170 MeV. The recoil deuteron energies in the Bates experiment ($q^2/2M_d$) were degraded by various materials (target wall, spectrometer windows, air, IFD detectors, and a carbon degrader for the runs taken at the two higher q points) between the liquid-deuterium target and the second dipole of the deuteron channel. The central deuteron energies were 133 MeV for the lowest q point and 160 MeV for the two higher q points as measured by a magnetic-field probe installed in the second dipole of the deuteron channel.

The yield for the scattering of polarized deuterons is given by [9]

$$N_C(\theta,\phi)=kN_0(\theta,\phi)[1+t_{20}T_{20}(\theta)+2t_{21}T_{21}(\theta)\cos(\phi)+2t_{22}T_{22}(\theta)\cos(2\phi)], \quad (2)$$

where N_0 is the yield for the scattering of unpolarized deuterons; t_{20}, t_{21}, and t_{22} are the tensor moments; T_{20}, T_{21}, and T_{22} are the analyzing powers; θ is the angle in the center-of-mass frame between the incident and outgoing tracks of the deuterons in the polarimeter; ϕ is the angle between the *e-d* and the *d-p* scattering planes; and k is an irrelevant normalization factor. The yield for the scattering of unpolarized deuterons and the analyzing powers were measured in the Saturne experiment, while in the Bates experiment the tensor polarization of the recoil deuterons was measured. The analyses for the calibration and the Bates data proceeded in the same way. The incident and outgoing tracks were reconstructed to determine the scattering vertices. The ΔE and E scintillators were gain matched to identify the particles detected in the polarimeter, and the angular distribution of detected protons was measured. A cut on the proton missing-energy spectrum ("E-diff cut") was applied to the data to eliminate highly inelastic protons coming from deuteron breakup reactions. The inclusion of some inelastic protons resulted in analyzing powers about 20% smaller than the values quoted above. In addition, because the deuteron energies incident on the polarimeter at Bates had large spreads, 14–23 MeV (full width at half maximum), and were not centered at any of the energies in the calibration experiment, the appropriate calibration was obtained by interpolation of the Saturne data using a Monte Carlo technique to simulate the energy and vertex position dependence of geometrical and absorption effects in the polarimeter. The actual incident deuteron spatial distributions of the Bates data were used to generate the interpolated-calibration data, while the energy distributions, not being measured accurately, were simulated using Gaussian distributions. The final results were found to be insensitive to reasonable changes in the above distributions.

TABLE I. Results of the t_{20} measurements.

q (fm^{-1})	θ_e (deg)	$t_{20}(q,\theta_e)$	$F_C(q)$	$F_Q(q)$
3.78 ± 0.02	80.9	$-1.24\pm0.17(0.10)$	$0.0127^{+0.0047}_{-0.0056}$	$0.482^{+0.077}_{-0.116}$
4.22 ± 0.02	78.7	$-0.82\pm0.15(0.11)$	$0.00166^{+0.00161}_{-0.00142}$	$0.315^{+0.010}_{-0.011}$
4.62 ± 0.02	76.7	$-0.41\pm0.18(0.13)$	$-0.00147^{+0.00106}_{-0.00104}$	$0.189^{+0.007}_{-0.008}$

The tensor moments were obtained using a fitting procedure which adjusted the t_{kq} in Eq. (2) such that the angular distribution of the interpolated-calibration data best reproduced the relative angular distribution of the Bates data. This procedure avoids the necessity for measuring the normalization factor k in the Bates experiment. The fitted values of t_{20} are given in Table I. The total uncertainties given in the table combine statistical and systematic uncertainties in quadrature, while the values in parentheses indicate the systematic uncertainties only. The systematic uncertainties are due to the E-diff cut, differences in the calibration of the CWC's between the Saturne and the Bates experiments, inexact knowledge of the deuteron energy spreads for the Bates kinematics, and the uncertainties in the interpolated-calibration data generated using the Monte Carlo simulation. In Table I, we also give the values of F_C and F_Q extracted from our measurements of t_{20} and from a parametrization [10] of the world data for the A and B structure functions. The extracted F_C and F_Q were obtained using a standard χ^2 minimization procedure. The uncertainties in F_C and F_Q correspond to a χ^2 change from $\chi^2_{\min}$ to $\chi^2_{\min}+1$. A change of 1 in χ^2 from its minimum value represents a 1-standard-deviation uncertainty.

The present results and previous t_{20} measurements are plotted in Fig. 2. They have been adjusted using $B(F_M)$, the extracted F_C and F_Q, and Eq. (1) to give the values for $\theta_e=70°$, the angle at which some of the theoretical curves shown in Fig. 2 were calculated. Those calculated in the Skyrme, six-quark, and perturbative quantum chromodynamics (PQCD) models are, however, for $\tilde{t}_{20}$. Setting $y=0$ in Eq. (1) lowers the value of t_{20} around the minimum by about 0.2.

An impulse-approximation (IA) prediction calculated using conventional nonrelativistic nuclear dynamics and a representative modern potential [Argonne V_{14} (AV_{14}) potential [11]] for the NN interaction is shown by the solid curve in Fig. 2. The addition of meson-exchange currents (MEC) results in a prediction (short-dashed curve) which clearly lies above the data for $q > 3.5$ fm^{-1}. Other IA calculation using various realistic NN potentials (Reid soft core, Bonn, Paris) [2] show similar features. On the other hand, the t_{20} prediction (double-dot-dashed curve) calculated using the new Bonn potential [12], which included an energy dependence in the potential and MEC contributions, is in good agreement with the data.

A recent relativistic one-boson-exchange prediction [13] of t_{20} gives reasonable agreement with the data and is similar to the nonrelativistic IA predictions. Other relativistic calculations using the formalism of light-cone quantum mechanics [14] also give predictions for t_{20} similar to those of nonrelativistic IA calculations.

Isobar degrees of freedom have been included in two coupled-channel (CC) models. In a model with very small $\Delta\Delta$ admixtures [15], the predicted t_{20} (long-dashed, curve) is in good accord with the data. The prediction of another CC model using a boundary-condition radius

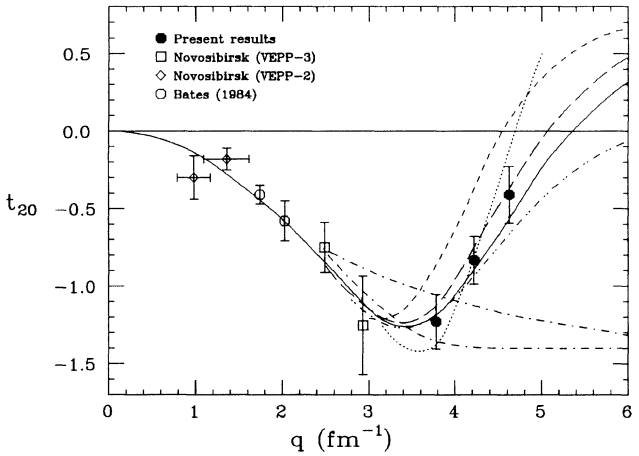

FIG. 2. Data and theoretical predictions of t_{20} as a function of four-momentum transfer. Data points: open circles, Ref. [3]; diamonds, Ref. [4]; squares, Ref. [5]; and solid circles, present results. All data points have been adjusted to give values for $\theta_e=70°$ (see text). The curves are predictions of different models (see text). (i) $\theta_e=70°$ in Eq. (1): IA+MEC AV_{14}, short-dashed curve (Ref. [11]); CC, long-dashed curve (Ref. [15]); IA AV_{14}, solid curve (Ref. [11]); new Bonn, double-dot-dashed curve (Ref. [12]). (ii) $y=0$ in Eq. (1): Skyrme, dotted curve (Ref. [19]); PQCD, dot-dashed curve (Ref. [20]); six-quark, dot-double-dashed curve (Ref. [18]).

[16] of $r_0=0.74$ fm lies above the data (not shown in Fig. 2) and is almost indistinguishable from the prediction of the IA+MEC calculation using the AV_{14} potential (short-dashed curve). Both CC models include MEC contributions, but it is noted that the t_{20} prediction for the CC model with $r_0=0.74$ fm agrees with the data if the MEC contributions are removed.

The predictions of several quark-cluster models [17], calculated using the resonating-group method and a quark-bag radius of about 0.5 fm, are all in qualitative agreement with the data. One quark description excluded by the present data is a simple six-quark prediction [18] (dot-double-dashed curve), in which a six-quark component was added directly to the deuteron wave function. In this model, the node in F_C is missing so that the predicted t_{20} remains negative for $q > 3$ fm^{-1}. Nonnucleonic effects are included in a totally different approach in the Skyrme model [19] where nucleons and nuclei are formed as topological solitons of pion and scalar meson fields. The value of t_{20} predicted by this model (dotted curve) is in reasonable agreement with the data. Finally, the prediction of the PQCD model [20] (dot-dashed curve) clearly fails to describe the data.

The present data unambiguously show a sharp rise of t_{20} from a minimum toward less negative values. This behavior is due to the node in F_C which is determined using a polynomial fit at $q=4.39\pm0.16$ fm^{-1}. The extracted values of F_C are plotted in Fig. 3 along with predictions for F_C, corresponding to the solid and short-

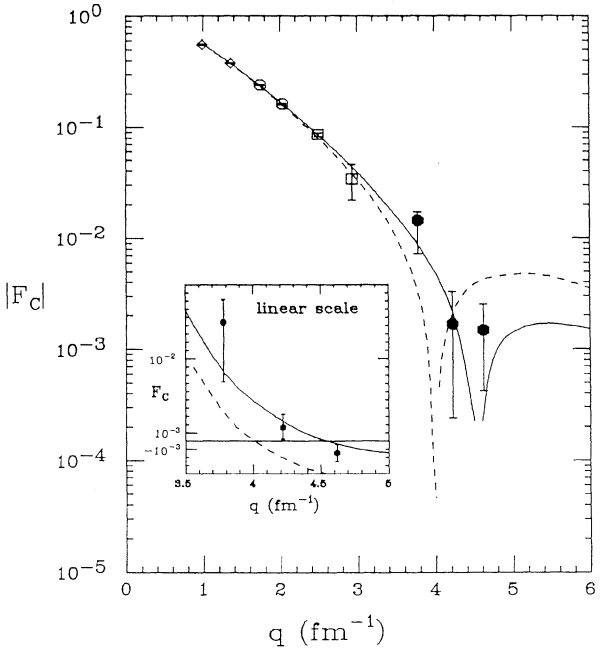

FIG. 3. Extracted F_C of the deuteron as a function of q. Same notations as in Fig. 2.

dashed curves in Fig. 2. As can be seen in Fig. 3, the nonrelativistic IA predictions [11] for F_C of the deuteron without MEC contributions is in good agreement with the data. However, this same nonrelativistic IA model [21] requires MEC contributions to give good agreement with the data for the form factors of the three- and four-body nuclei.

We gratefully acknowledge assistance from L. Antonuk, J. Pasos, G. van der Steenhoven, and A. J. Wagner. We also thank the Bates staff for their help in mounting and running this experiment. This work was supported by the U.S. Department of Energy under Contract No. DE-AC02-76ER03069, the National Science Foundation, the Natural Sciences and Engineering Research Council of Canada, and NATO Collaborative Research Grant No. 860669.

[1] R. G. Arnold *et al.*, Phys. Rev. Lett. **35**, 776 (1975); S. Auffret *et al.*, *ibid.* **54**, 649 (1985); P. E. Bosted *et al.*, Phys. Rev. C **42**, 38 (1990); S. Platchkov *et al.*, Nucl. Phys. **A510**, 740 (1990).
[2] M. I. Haftel, L. Mathelitsch, and H. F. K. Zingl, Phys. Rev. C **22**, 1285 (1980).
[3] M. E. Schulze *et al.*, Phys. Rev. Lett. **52**, 597 (1984).
[4] V. F. Dmitriev *et al.*, Phys. Lett. **157B**, 143 (1985); B. B. Voitsekhovskii *et al.*, Pis'ma Zh. Eksp. Teor. Fiz. **43**, 567 (1986) [JETP Lett. **43**, 733 (1986)].
[5] R. Gilman *et al.*, Phys. Rev. Lett. **65**, 1733 (1990).
[6] M. Garçon *et al.*, Nucl. Phys. **A458**, 287 (1986); E. J. Stephenson *et al.*, Indiana University Cyclotron Facility Scientific and Technical Report No. 58, 1983 (unpublished).
[7] J. Arvieux *et al.*, Nucl. Instrum. Methods Phys. Res., Sec. A **273**, 48 (1988).
[8] J. M. Cameron *et al.* (to be published).
[9] R. G. Arnold, C. E. Carlson, and F. Gross, Phys. Rev. C **23**, 363 (1981).
[10] S. Platchkov (private communication).
[11] R. Schiavilla and D. O. Riska, Phys. Rev. C **43**, 437 (1991).
[12] J. Pauschenwein, L. Mathelitsch, and W. Plessas (to be published).
[13] E. Hummel and J. A. Tjon, Phys. Rev. Lett. **63**, 1788 (1989); Phys. Rev. C **42**, 423 (1990).
[14] P. L. Chung, F. Coester, B. D. Keister, and W. N. Polyzou, Phys. Rev. C **37**, 2000 (1988); L. L. Frankfurt, I. L. Grach, L. A. Kondratyuk, and M. I. Strikman, Phys. Rev. Lett. **62**, 387 (1989).
[15] R. Dymarz and F. C. Khanna, Nucl. Phys. **A507**, 560 (1990); Phys. Rev. C **41**, 2438 (1990).
[16] W. P. Sitarski, P. G. Blunden, and E. L. Lomon, Phys. Rev. C **36**, 2479 (1987); P. G. Blunden, W. R. Greenberg, and E. L. Lomon, *ibid.* **40**, 1541 (1989).
[17] Y. Yamauchi and M. Wakamatsu, Nucl. Phys. **A457**, 621 (1986); H. Ito and A. Faessler, *ibid.* **A470**, 626 (1987); H. Ito and L. S. Kisslinger, Phys. Rev. C **40**, 887 (1989).
[18] V. V. Burov and V. N. Dostovalov, Z. Phys. A **326**, 245 (1987).
[19] E. M. Nyman and D. O. Riska, Nucl. Phys. **A468**, 473 (1987).
[20] C. E. Carlson, Nucl. Phys. **A508**, 481c (1990).
[21] R. Schiavilla, V. R. Pandharipande, and D. O. Riska, Phys. Rev. C **40**, 2294 (1989); **41**, 309 (1990).